International Journal of Heat and Fluid Flow 30 (2009) 108–116

Contents lists available at ScienceDirect

International Journal of Heat and Fluid Flow

journal homepage: www.elsevier.com/locate/ijhff

# A study on the fuel injection and atomization characteristics of soybean oil methyl ester (SME)

Su Han Park, Hyung Jun Kim, Hyun Kyu Suh, Chang Sik Lee *

*Graduate School of Hanyang University, Department of Mechanical Engineering, Hanyang University, 17 Haengdang-dong, Sungdong-gu, Seoul 133-791, Republic of Korea*

ARTICLE INFO

*Article history:*
Received 11 July 2008
Received in revised form 31 October 2008
Accepted 3 November 2008
Available online 21 December 2008

*Keywords:*
SME (soybean oil methyl ester)
Atomization
Sauter mean diameter (SMD)
Kelvin–Helmholtz breakup model
Rayleigh–Taylor model
Spray tip penetration

ABSTRACT

The spray atomization characteristics of an undiluted biodiesel fuel (soybean oil methyl ester, SME) in a diesel engine were investigated and compared with that of diesel fuel (ultra low sulfur diesel, ULSD). The experimental results were compared with numerical results predicted by the KIVA-3V code. The spray characteristics of the spray tip penetration, spray area, spray centroid and injection delay were analyzed using images obtained from a visualization system. The Sauter mean diameter (SMD) was analyzed using a droplet analyzer system to investigate the atomization characteristics.

It was found that the peak injection rate increases and advances when the injection pressure increases due to the increase of the initial injection momentum. The injection rate of the SME, which has a higher density than diesel fuel, is higher than that of diesel fuel despite its low injection velocity. The high ambient pressure induces the shortening of spray tip penetration of the SME. Moreover, the predicted spray tip penetration pattern is similar to the pattern observed experimentally. The SMD of the SME decreases along the axial distance. The predicted local and overall SMD distribution patterns of diesel and SME fuels illustrate similar tendencies when compared with the experimental droplet size distribution patterns.



## 1. Introduction

The combustion and exhaust emissions characteristics of a diesel engine are affected by fuel spray and atomization characteristics, as well as by fuel properties. Therefore, the improvement of thermal efficiency and reduction of exhaust emissions were achieved through the optimizations of fuel spray characteristics, including spray tip penetration, spray area, and droplet size. The common-rail injection system with high injection pressure is more advantageous than the conventional injection system in this regard, as it has a better fuel atomization performance, a short injection duration, free control of the injection timing and injection duration. The main factors that affect the fuel spray and atomization characteristics are the injection pressure, split injection, injection duration and nozzle cavitation. Split injection is the injection strategy which an amount of single injection was divided into equal halves, injected individually. These factors have been investigated in previous studies (Park et al., 2008; Payri et al., 2004; Song et al., 2005), and the relationship between combustion and emission characteristics and spray and atomization characteristics have been expound upon by many researchers (Park et al., 2003; Yi et al., 2003).

Biodiesel is a promising alternative fuel from an environmental perspective. Moreover, biodiesel fuel can be used in a diesel engine without modification of the fuel supply system. Therefore, investigations of the spray combustion and emissions characteristics of diesel–biodiesel blended fuel are ongoing.

Suh et al. (2008) reported on the spray and combustion characteristics as a function of the blending ratio of diesel and biodiesel fuel under various injection conditions, such as single and pilot injection. The pilot injection strategy can be achieved by the injection of a small amount of fuel shortly before the start of main injection. They showed that the atomization and combustion performances were improved by using pilot injection, and CO and HC emissions decreased as a result of the enhanced fuel atomization. They also found that $NO_x$ emission was increased by high temperatures in the combustion chamber, caused by heat released when the pilot injection timing approaches the main injection timing. Kim et al. (2008) studied the effect of split injection on exhaust emissions, soot particulate, and engine performance of biodiesel fuel. They reported that split injection reduced $NO_x$ emissions significantly without a significant increase of soot emission.

Lee et al. (2005) investigated the combustion and emission characteristics of biodiesel-diesel blended fuels. They reported that as the blending ratio of the biodiesel fuel is increased, HC and CO emissions decreased, while $NO_x$ emission increased. This behavior is attributed to the increase of the combustion temperature promoted by the oxygen in the biodiesel fuel.

* Corresponding author. Tel.: +82 2 2220 0427; fax: +82 2 2281 5286.
*E-mail address:* cslee@hanyang.ac.kr (C.S. Lee).

0142-727X/$ - see front matter © 2008 Elsevier Inc. All rights reserved.
doi:10.1016/j.ijheatfluidflow.2008.11.002

**Nomenclature**

| | | | |
|---|---|---|---|
| $D$ | nozzle hole diameter (mm) | $T_f$ | fuel temperature (K) |
| KH | Kelvin–Helmholtz | $t_{asoi}$ | time after start of injection (ms) |
| $L_Z$ | the axial distance along the spray axis (mm) | $t_{eng}$ | energizing duration (ms) |
| $P_{amb}$ | ambient pressure (MPa) | $\rho_f$ | fuel density (kg/m$^3$) |
| $P_{inj}$ | injection pressure (MPa) | $\rho_g$ | ambient gas density (kg/m$^3$) |
| RT | Rayleigh–Taylor | $\sigma$ | surface tension (N/m) |

Hong et al. (2003) compared the spray characteristics of diesel and biodiesel fuel using high pressure fuel injection. They found that the spray tip penetration of biodiesel fuel is greater than that of diesel, but the spray cone angle is less than that of diesel. They also reported that the decrease in the spray angle is related to the increased spray tip penetration. Besides, Kegl et al. (2008) and Schonborn et al. (2008) investigated the optimal fuel injection system and the effect of the molecular structure on the $NO_x$ and P.M. (particulate matter) formation of biodiesel fuel, respectively.

While there have been many studies investigating the spray and combustion characteristics of diesel–biodiesel blends, there have been relatively few studies that have focused on spray and atomization characteristics of an undiluted biodiesel fuel. In this study, the spray and atomization characteristics of an undiluted biodiesel fuel derived from soybean oil were compared with those of diesel fuel. The spray and atomization characteristics of biodiesel fuel such as fuel injection rate, spray tip penetration and spray cone angle, the centroid of spray, spray evolution process, spray droplet size, and velocity, were compared with results predicted using a theoretical method. The breakup model for the simulation of the diesel and biodiesel fuel spray consisted of a primary breakup (Kelvin–Helmholtz model) and a secondary breakup (Rayleigh–Taylor model).

## 2. Numerical model

### 2.1. Applied biodiesel fuel in the calculation code

In order to apply the diesel and biodiesel fuel in the KIVA-3V code, the DF2 (diesel fuel No. 2) from the fuel library was used to calculate the diesel sprays. The fuel library in the KIVA-3V code needs to calculate the fuel properties. This basic information of fuel is molecule weight, critical temperature, and fuel properties such as density of liquid phase, the liquid viscosities, and surface tension according to the temperature. Yoon et al. (2008) studied fuel properties such as the density, dynamic viscosity, and kinematic viscosity of biodiesel and diesel–biodiesel blended fuels as a function of the fuel temperature. These results have been added to the fuel library in the calculation.

### 2.2. KH breakup and RT breakup model

The prediction of the spray characteristics of biodiesel and diesel was performed using a hybrid breakup model combining two different models: the Kelvin–Helmholtz (KH) model for the primary breakup and the Rayleigh–Taylor (RT) model for the secondary breakup. This hybrid model was suggested by Su et al. (1996). In this study, the breakup length $L_b$ was calculated from the equation proposed by Beale and Reitz (1999).

$$L_b = \frac{1}{2} B_1 D \sqrt{\frac{\rho_f}{\rho_g}} \tag{1}$$

where $B_1$ is the breakup constant of the KH model, which was determined to be 40 after the comparison between the experimental and calculated results. For the numerical analysis, the calculations of spray behaviors and atomization were conducted on equal terms with the experimental conditions. It is assumed that the initial diameter of injected droplet at the injector exit is equal to the nozzle hole diameter. In addition, the initial time interval 20 μs and the computational grid with 2-dimensional grid 100 mm in width and 500 mm in length was created to prevent the impingement on bottom wall during the calculation time. Number of cells is about 39,000 cells. The calculation grid with 2 mm of the grid cell size in both width and height was determined by grid sensitivity study as illustrated in Fig. 1. Primary breakup principally occurs due to KH instability until the breakup length and the breakup of droplet is governed by only RT model at the lower part of breakup length.

Reitz (1987) suggested the KH breakup model on the basis of a Kelvin–Helmholtz instability analysis of a liquid jet. This model considers the effect of wave instability on the liquid surface. The maximum growth rate $\Omega_{KH}$ and the corresponding wavelength ($\Lambda_{KH}$) can be calculated from the solution of the dispersion relation equation.

Assuming the droplet radius decreases the critical radius ($r_c$) during the breakup process the droplet radius after the breakup ($r_n$) can be calculated using the following equation

$$\frac{r - r_n}{dt} = \frac{r - r_c}{\tau_{KH}} \tag{2}$$

where the critical radius and breakup time are $r_c = 0.61\Lambda_{KH}$ and $\tau_{KH}$, respectively.

The frequency of the fast growing RT wave ($\Omega_{RT}$), the corresponding wavelength ($\Lambda_{RT}$), and wave number ($K_{RT}$), the breakup time ($\tau_{RT}$) and the radius ($r_c$) after breakup were determined via Rayleigh–Taylor instability (Bellman and Pennington, 1954). After

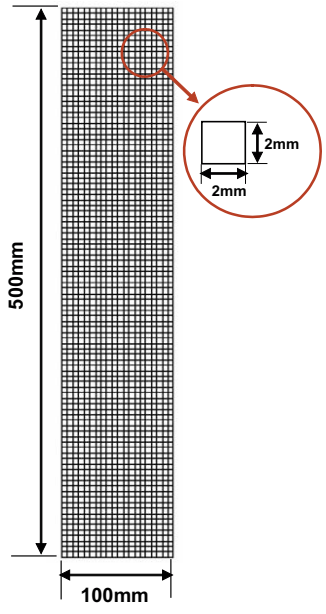


**Fig. 1.** Computation grid for the numerical analysis.

the wave stops growing, the breakup time ($\tau_{RT}$) elapses and the breakup of small droplets occurs. The breakup time of the RT model and the radius ($r_c$) after the breakup are defined by

$$\tau_{RT} = C_\tau/\Omega_{RT}, \quad r_c = \pi C_{RT}/K_{RT} \tag{3}$$

where, breakup constants $C_{RT}$ and $C_\tau$ are set to the optimal values of 0.1 and 1.0, respectively, after the comparison of theoretical and experimental results.

## 3. Experimental apparatus and procedure

### 3.1. Test injector and fuel properties

A test injector with a single hole nozzle 0.3 mm in diameter and 0.8 mm in orifice length was used for spray visualization and measurement of droplet size, as shown in Fig. 2. The test injector was controlled by a peak current of 21.0 A and a hold current of 11.0 A. The injector driver and a time delay/pulse generator controlled the injection timing and duration of the spray, respectively.

The spray and atomization characteristics were investigated with respect to injection and ambient conditions using an undiluted biodiesel fuel derived from soybean oil. Experimental results were concurrently compared with the numerical results, and the spray characteristics of the biodiesel fuel were compared with those of the diesel fuel. The properties of diesel and biodiesel fuel are shown in Table 1.

### 3.2. Injection rate measuring system

The fuel injection rate is one of the most important factors to measure because it is used in the design of injection systems and combustion chambers. The injection rates of the diesel and biodiesel fuels were measured and analyzed using an injection rate measuring system based on the Bosch method (Bosch, 1966), in which the pressure variation in a tube is monitored as fuel is injected into the tube. In this experiment, the pressure in the tube was set to 4.0 MPa. This system was used to determine the time resolved injection profile, and the injection rates of both fuels were compared to each other. A diagram of the calculations is shown in Fig. 3.

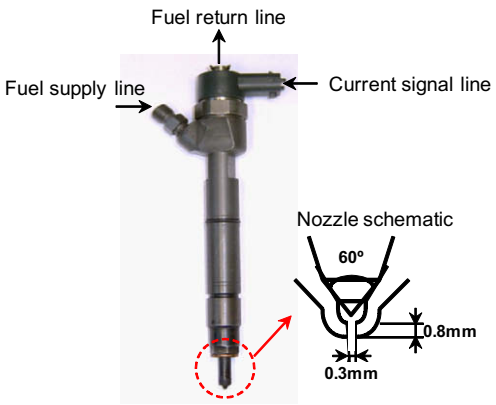


**Fig. 2.** Test injector and single hole nozzle.

**Table 1**
Fuel properties of diesel and biodiesel fuels.

| Fuel properties (20 °C) | Diesel | Biodiesel |
|---|---|---|
| Fuel density (kg/m$^3$) | 822 | 870 |
| Dynamic viscosity (mPa s) | 3.22 | 6.05 |
| Kinematic viscosity (mm$^2$/s) | 3.917 | 6.954 |

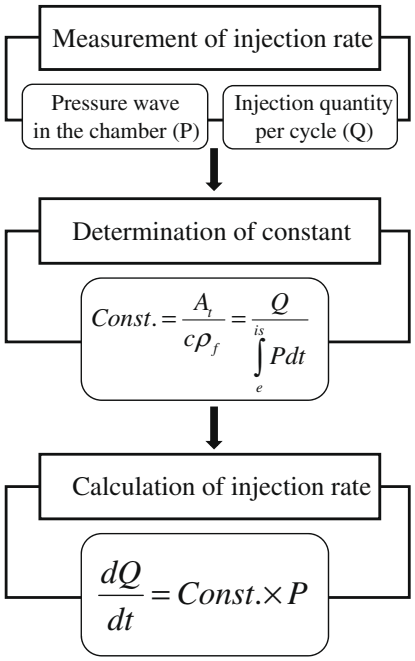


**Fig. 3.** Flow chart of the experimental procedure to determine the injection rate.

A piezo pressure sensor (KISTLER, 601A) was used to measure the pressure variation in the tube. The injection rate meter included an adapter, a measuring tube 5 m in length, a pressure vessel, a relief valve and a throttle valve. A data acquisition board (National Instrument, NI6013) was used for the acquisition of injection profiles, and the injection quantity was obtained from the mean value of 1000 continuous injections.

### 3.3. Visualization and droplet measuring system

Fig. 4 shows a schematic of the visualization and droplet measuring system used to capture the spray images and obtain the droplet size and velocity. In both systems, the fuel supply system consisted of a high pressure pump (Haskel, HSF-300), a common-rail injector, and an injector driver (TEMS, TDA-3200). The spray visualization system was composed of a Nd:YAG laser (Continum, SL2-10), a set of cylindrical lenses and mirrors, a digital delay/pulse generator

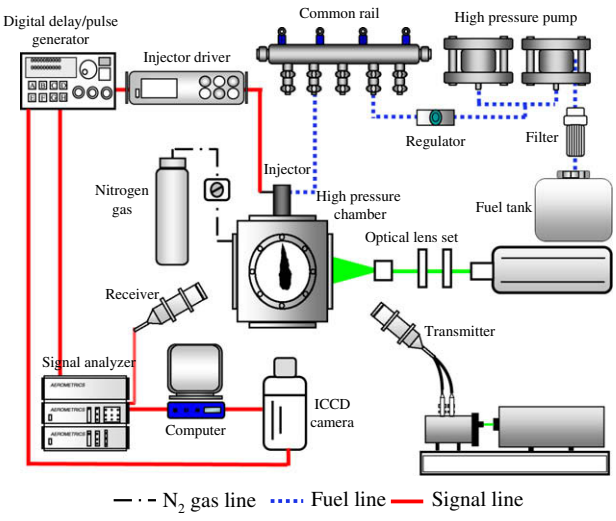


**Fig. 4.** Schematic of the visualization system and the droplet measuring system.

(Berkeley Nucleonics Corp., Model 555), a high resolution ICCD (intensified charge coupled device) camera (The Cooke Corporation, Dicam-PRO), and a PC-installed an image grabber. The Nd:YAG laser light source has a 532 nm wave length. The spray was illuminated by the cylindrical lenses, which form a laser sheet beam less than 1mm. The injector driver, the exposure time of the ICCD camera, and the oscillation signal of the Nd:YAG laser were synchronized using the digital delay/pulse generator. The high pressure chamber was pressurized by nitrogen gas. Detailed specifications of the Nd:YAG laser and the ICCD camera are shown in Table 2.

The droplet measuring system (phase Doppler particle analyzer, PDPA) shown in Fig. 4 was used to analyze the droplet size of the diesel and biodiesel fuel. The laser output and PMT (photomultiplier tube) voltage were set to 700 mW and 500 V, respectively, based on the data acquisition rate and signal intensity. When fuel droplets pass through the measurement volume of fringe created by the laser beam from the Ar-ion laser (INNOVA 70 C, Coherent), the dispersed beam is detected at the receiver. The detected phase difference and Doppler signal frequency are then converted to the mean droplet size and velocity. Detailed specifications of the PDPA system are shown in Table 3.

### 3.4. Experimental

The injection rate profile, spray area and spray centroid variation were measured and analyzed to study the macroscopic spray characteristics. The spray tip penetration was defined as the maximum distance from the nozzle tip reached by the injected spray. The fuel droplet size was obtained from the PDPA system for the analysis of the fuel atomization. Spray droplets were measured every 5 mm from 5 mm to 70 mm along the axial direction and every 2 mm from 2 mm to 10 mm along the radial direction at 40 mm, 50 mm, and 60 mm from the spray axis. The cut-off range for droplet measurement using the droplet measuring system was set from 2 μm to 70 μm, and approximately 20,000 spray droplets were averaged at each measuring point. In this work, fuel temperature and the ambient air temperature of high pressure chamber in visualization system are 20 °C. In addition, the droplet measurement experiment was conducted at room temperature.

## 4. Results and discussions

### 4.1. Injection rate profile

The injection rate profile plays an important role in the analysis of the performance of a fuel injector, because it is used to determine the injection delay and transient mass flow rate. In addition, the injection rates are used to calculate the input parameters to the program, mainly the initial velocity and SMD (Sauter mean diameter). The effects of the injection pressure and energizing duration on the injection rate profile of biodiesel fuel were studied using Bosch method (Bosch, 1966).

Fig. 5a shows the injection rate profile of biodiesel fuel at various injection pressures. When the injection pressure increases, the peak injection rate also increases, and the peak injection rate occurs earlier. This result indicates that the high-pressure in the mini-sac, defined as the space between the injector needle tip and the inside wall of injector, causes a high injection velocity early in the injection stage. The rapid pressure drop causes the injection rate profile to approach that of spray injected at a lower pressure late in the injection stage (Park, 2005).

The effect of the energizing duration on the injection rate profile of biodiesel fuel while the injection and ambient pressure conditions were held constant is illustrated in Fig. 5b. With the same injection pressure, the injection momentum, which affects the initial spray behavior, is almost the same regardless of the energizing duration. Hence, the injection rate profile has the same gradient. In the case of $t_{eng}$ = 0.3 ms, the injection rate profile was unstable,

**Table 2**
Specification of the Nd:YAG laser and the ICCD camera.

| | | |
|---|---|---|
| Nd:YAG laser (light source) | Wave length | 532 nm |
| | Laser power | 270 mJ (max) |
| | Beam thickness | ~1.0 mm |
| ICCD camera | Pixel size | 6.7 μm × 6.7 μm |
| | Scan area | 8.6 mm × 6.9 mm |
| | Resolution | 1280 (H) × 1024 (V) |

**Table 3**
Specification of the PDPA system.

| | |
|---|---|
| Light source | Ar-ion laser |
| Wave length | 514.5 nm, 488 nm |
| Laser beam diameter | 1.4 mm |
| Focal length | 250 mm for transmitter and receiver |
| Collection angle | 30° |
| PMT voltage | 500 V |

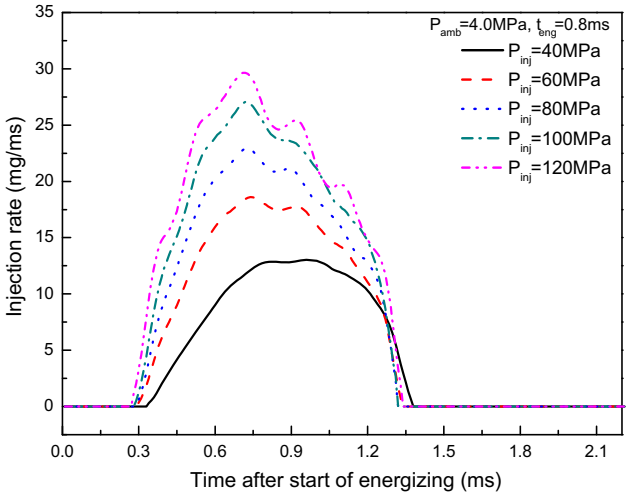


(a) Effect of the injection pressure

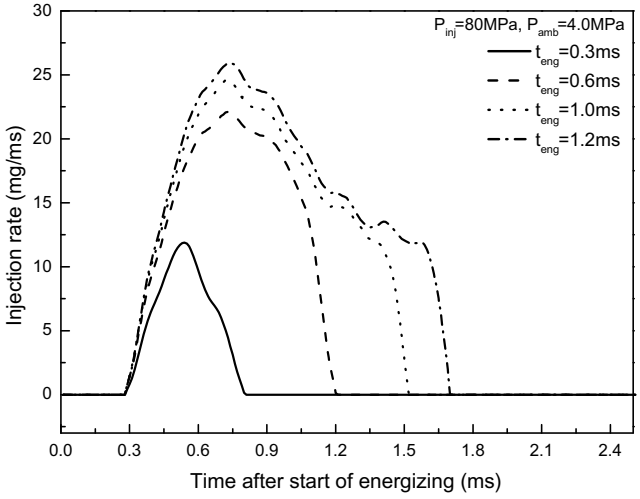


(b) Effect of the energizing duration

**Fig. 5.** Injection rate profile of biodiesel fuel ($P_{amb}$ = 4.0 MPa, $t_{eng}$ = 0.8 ms).

because the energizing duration was less than the timing of the peak current ($t_{peak}$ = 0.4 ms).

Fig. 6 shows the injection delay and the real injection duration, which can be analyzed from the results of Fig. 5a. Injection delay is defined as the time interval between the start of energizing and the initial increase in the injection rate, and the real injection duration is defined as the period of the fuel is delivered through the injector which is indicated by the injection rate, not the energizing duration. When the injection pressure increased from 40 MPa to 120 MPa, the injection delay decreased from 0.33 ms to 0.27 ms. It is said that the increased fuel momentum by the increase of the injection pressure causes the rapid opening of the needle, and enables to easily overcome the friction between the fuel and nozzle wall. Moreover, the real injection duration indicated 1.04 ms that is 30% longer than the energizing duration of the injector. It can be confirmed that the real injection duration becomes longer than the energizing duration ($t_{eng}$ = 0.8 ms) due to the response time of the injector solenoid for the input signal from the injector driver.

Fig. 7 shows the comparison of the volumetric injection rate and injection velocity between diesel and biodiesel fuel under an energizing duration of 1.2 ms. Injection velocities of diesel and biodiesel fuel were obtained from the nozzle flow model suggested by Sarre et al. (1999). As shown in Fig. 7a, the volumetric injection rate of biodiesel fuel is lower than that of diesel fuel, totally. The peak volumetric injection rate of biodiesel fuel is higher than that of diesel fuel. Additionally, as shown in Fig. 7b, the lower injection velocity of biodiesel fuel causes the lower volumetric injection rate. On the other hand, the increase of injection pressure leads the increase of the peak injection rate, due to the increase of the initial spray momentum.

### 4.2. Spray penetration, spray area, and centroid variation

Fig. 8 shows the effect of the ambient pressure and the injection pressure on the spray tip penetration of diesel and biodiesel fuel, determined experimentally and numerically. Because of higher ambient gas density, the spray tip penetration decreases as the ambient pressure increases. It can be postulated that at a higher ambient pressure, the leading edge of the spray was decelerated by the higher ambient gas density, causing the spray tip to develop slowly. Due to the higher injection momentum, the tip penetration increases as the injection pressure increases. The magnitude and shape of spray tip penetration of diesel and biodiesel fuel are almost the same, as determined both experimentally and numerically. As the time after the start of injection increases, the difference between the spray tip penetration of both fuels increases a little. Diesel fuel mixed more actively with the ambient gas as compared to biodiesel fuel, which has a higher kinematic viscosity. Moreover, the spray penetrating region could be divided in two: the main region of the spray and the front edge of the spray. The main region of the spray is governed by the inertia of the injection liquid spray and the momentum of the entrained ambient air. In contrast, the front edge of the spray is governed by the inertia of the droplets delivered from the main region, as well as by the aerodynamic drag force (Roisman et al., 2007). It follows then, that after completion of the injection, the spray was mainly affected by the aerodynamic drag force. The theoretical results obtained for biodiesel fuel are in the good agreement with the experimental results at the lower ambient pressure, whereas at a higher ambient pressure, there is some difference between the numerical and experimental results. Percent errors between experimental and numerical results are about 2.8–4.8%. However, these differences, with a maximum 6 mm are considered negligible.

Fig. 9 shows the comparison between the experimental images obtained through the visualization system and the numerical spray process developed using the hybrid breakup model of diesel and biodiesel fuel at 1.3 ms after the start of the injection. When the

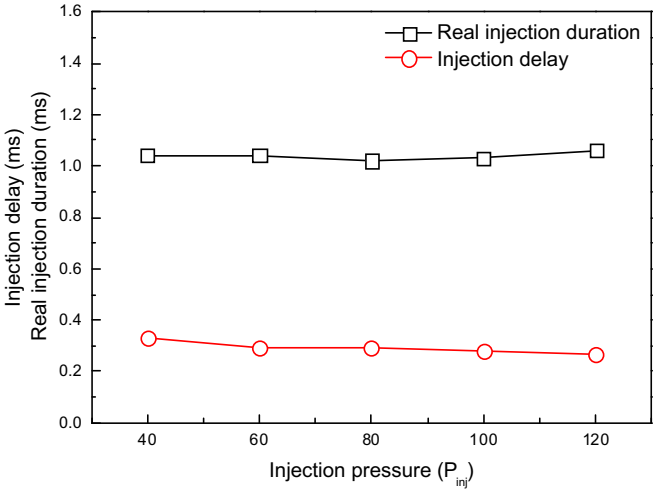


**Fig. 6.** Effect of the injection pressure on the injection characteristics ($P_{amb}$ = 4.0 MPa, $t_{eng}$ = *0.8 ms*).

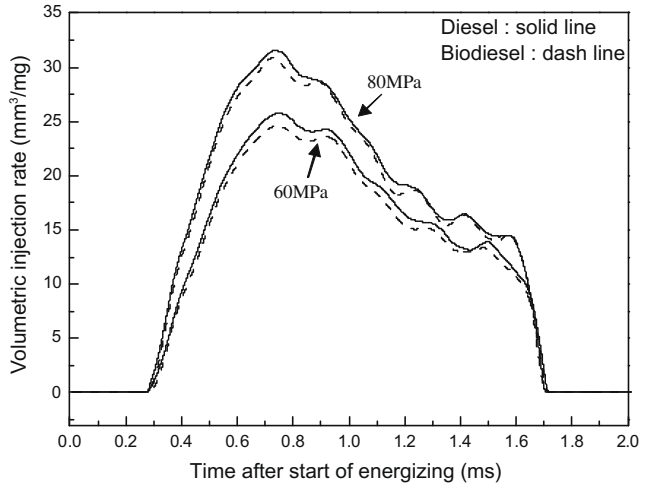


(a) Injection rate

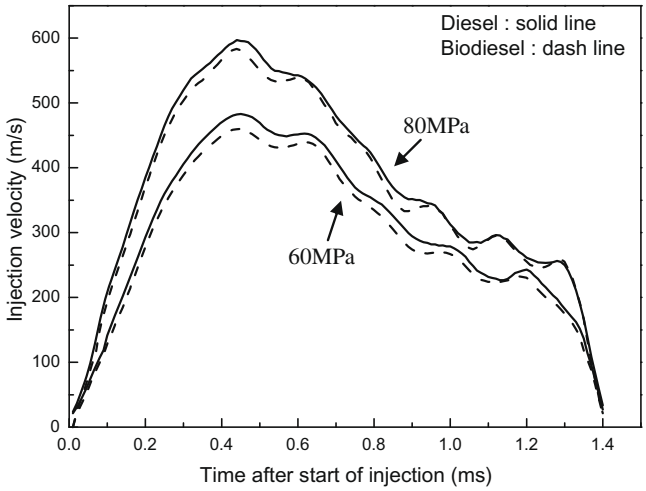


(b) Injection velocity

**Fig. 7.** Comparison of the volumetric injection rate and velocity between diesel and biodiesel fuels ($t_{eng}$ = 1.2 ms, $P_{amb}$ = 4.0 MPa).

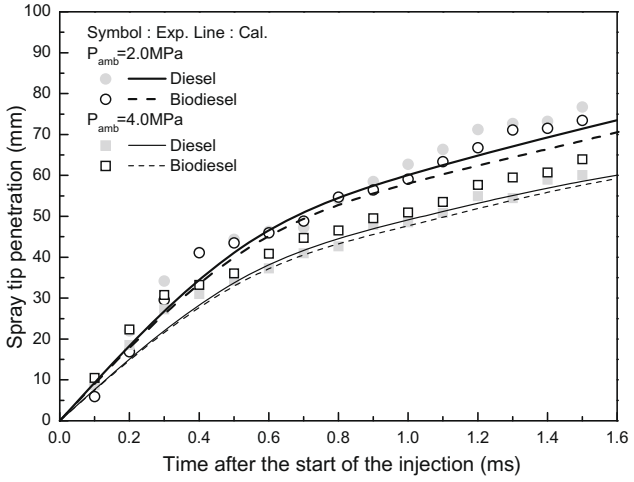


(a) $P_{inj}$=60MPa

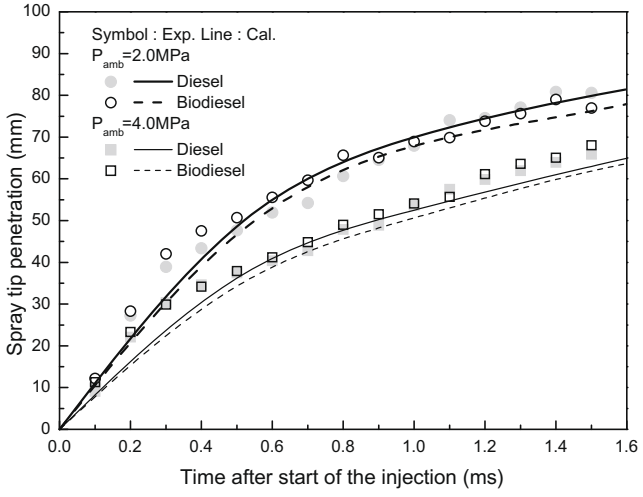


(b) $P_{inj}$=80MPa

**Fig. 8.** Comparison between the experimental and numerical results of diesel and biodiesel fuels ($t_{eng}$ = 1.2 ms, $T_f$ = 293 K).

ambient gas pressure increased from 2 MPa to 4 MPa, it was observed that the spray images of diesel and biodiesel fuel from the experiment and from the numerical calculations got shorter. Moreover, the numerical results showed that the vortex, which was formed downstream of the spray, became faint due to the active mixing of the injected fuel and ambient gas, caused by the increase in ambient gas pressure. In addition, biodiesel fuel with a high viscosity has fewer droplets due to the breakup frequency, which is relatively low compared to that of diesel fuel at the spray edge. As shown in Fig. 9, the numerical results indicated on the right side of the spray axis show a similar pattern to those seen in experimental images.

In this work, the spray area and the spray centroid of biodiesel fuel were investigated and compared with those of diesel fuel. The goal was to gain an understanding of the distribution of the injected fuel, as well as to explore the effects of the ambient pressure on the system. The spray areas and the spray centroids were calculated using image threshold processing (threshold value = 190).

Fig. 10 illustrates the effect of the ambient pressure on the spray area distribution and the spray centroid variation (on the *Y*-axis) of biodiesel fuel. The spray area increases linearly as time elapses after the start of injection, as shown in Fig. 10a. Moreover, as the ambient pressure increases, the gradient in the spray area distribution tapers off, as shown in Fig. 10a. It was confirmed that the spray tip penetration decreases with increasing ambient pressure, as shown in Fig. 8. In addition, the spray centroid (shown on the *Y*-axis) decrease slowly as the ambient pressure increases, as illustrated in Fig. 10b. It is postulated that the spray propagation was resisted by the higher density of the ambient gas.

### 4.3. Local and overall droplet size distribution of biodiesel fuel

The Sauter mean diameter (SMD) is the ratio of the volume to surface area. The SMD is commonly used, because it characterizes a number of important processes involving drop penetration and heat and mass transfer (Bayvel and Orxechowski, 1993).

In this investigation, the local and overall droplet sizes of the biodiesel fuel were measured using the PDPA system. These droplet sizes were compared with those of diesel fuel. The experimental results were compared with the numerical results calculated using KIVA-3V.

Fig. 11 shows the comparison between the experimental and numerical results for the droplet size distribution of diesel and biodiesel fuel. In this figure, symbols indicate the experimental results and the lines with symbols indicate the calculated results. The experimental results were obtained under the following conditions: injection pressure of 60 MPa, ambient pressure of 0.1 MPa, and an energizing duration of 1.2 ms. As shown in Fig. 11, the patterns of the predicted local and overall SMD distribution agree reasonably well with the experimental results of biodiesel fuel. Also, the droplet size of the biodiesel fuel from the experimental results

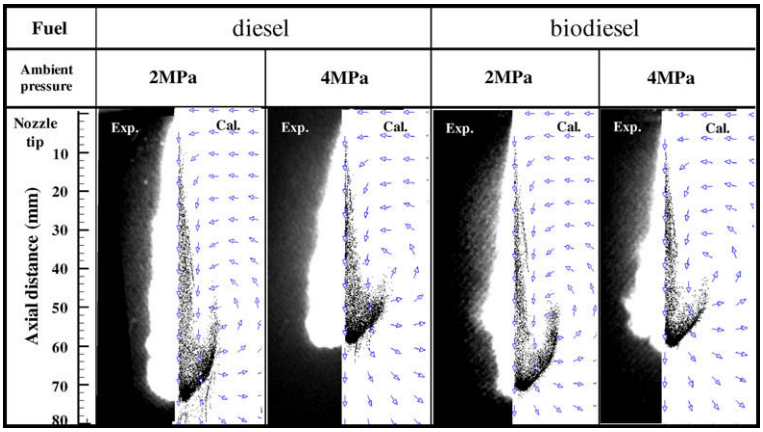


**Fig. 9.** Comparison of the experimental and calculated spray images of diesel and biodiesel fuels according to ambient pressure ($P_{inj}$ = 80 MPa, $t_{eng}$ = 1.2 ms, $t_{asoi}$ = 1.3 ms).

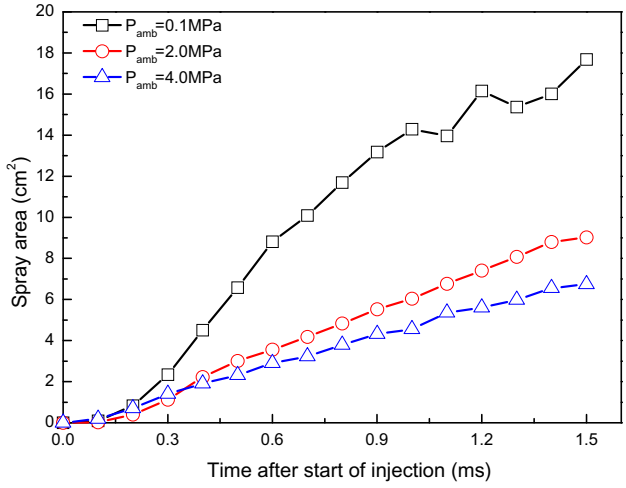


(a) Spray area

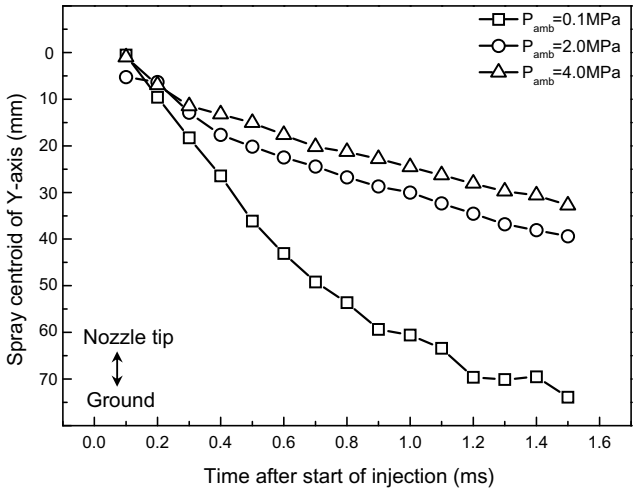


(b) Spray centroid of Y-axis

**Fig. 10.** Effect of the ambient pressure on the spray area distribution and the spray centroid of biodiesel fuel ($P_{inj}$ = 60 MPa, $t_{eng}$ = 1.2 ms).

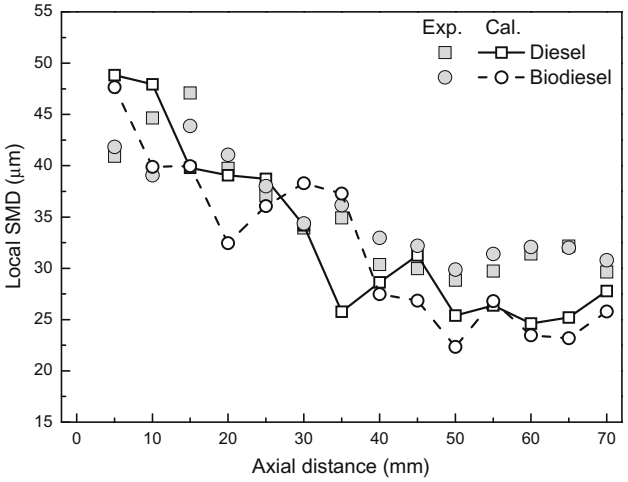


(a) Local Sauter mean diameter ($D_{32}$)

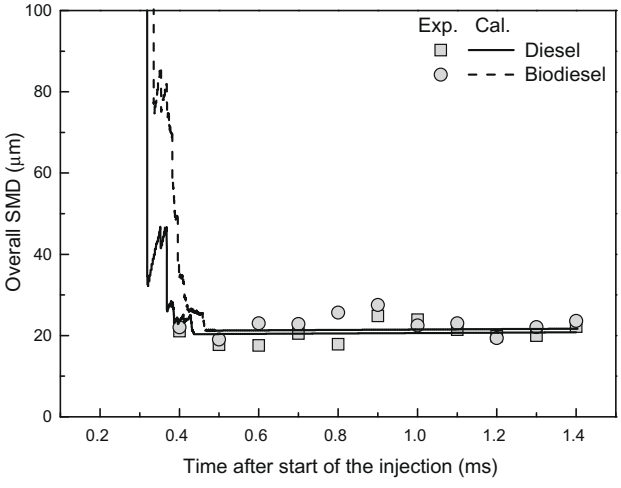


(b) Overall SMD

**Fig. 11.** Comparison of the experimental and numerical results on the droplet size distribution of diesel and biodiesel fuel ($P_{inj}$ = 60 MPa, $P_{amb}$ = 0.1 MPa, $t_{eng}$ = 1.2 ms).

is a little larger than that of diesel fuel. One of important factors which affect the fuel atomization is a viscosity coefficient (Ejim and Fleck, 2007). Biodiesel fuel has higher viscosity than a diesel fuel. In addition, it is postulated that the worse volatility characteristic of biodiesel fuel affected a bad atomization of spray performance compared to diesel fuel. Therefore, it is said that biodiesel fuel blended with other fuels which had low viscosity and good volatility results in the improvement of fuel injection and atomization characteristics in a diesel engine. On the other hand, the droplet size of biodiesel fuel decreases along the axial distance. This was confirmed in Fig. 12, which shows the detected droplet percentage of biodiesel fuel as a function of the droplet size distribution with $L_Z$ = 20 mm and $L_Z$ = 50 mm ($L_Z$: the distance from the nozzle tip). The detected droplet percentage was obtained from the ratio of the number of droplets each point to the total number of detected droplets. As seen in Fig. 12, the droplets atomize due to the interaction between the spray and the ambient gas when the spray moves downstream.

Fig. 13 shows the overall mean droplet size distribution of diesel and biodiesel fuel in the form of a contour plot. The droplet size distributions were measured from 40 mm to 60 mm for the axial direction and 8 mm for the radial direction. As shown in Fig. 13, $D_{10}$ (AMD, Arithmetic mean diameter) and $D_{32}$ (SMD) for biodiesel

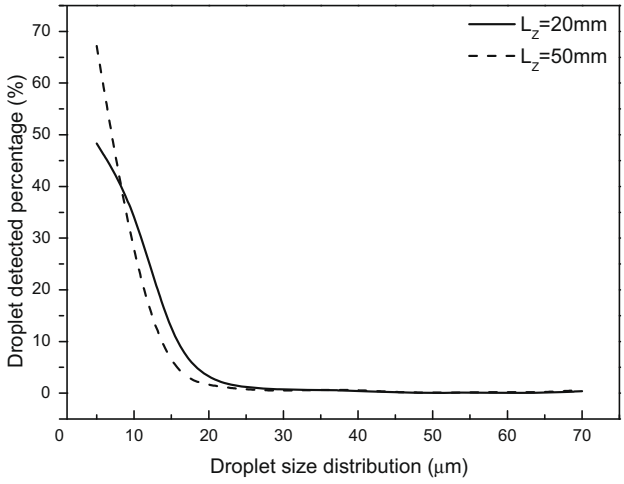


**Fig. 12.** Droplet detected percentage of biodiesel fuel at $L_Z$ = 20 mm and $L_Z$ = 50 mm ($P_{inj}$ = 60 MPa, $P_{amb}$ = 0.1 MPa, $t_{eng}$ = 1.2 ms).

fuel represented the higher values due to the higher kinematic viscosity. The SMD of both fuels decreases smoothly in the radial direction. In addition, the SMD of biodiesel fuel shows the de-

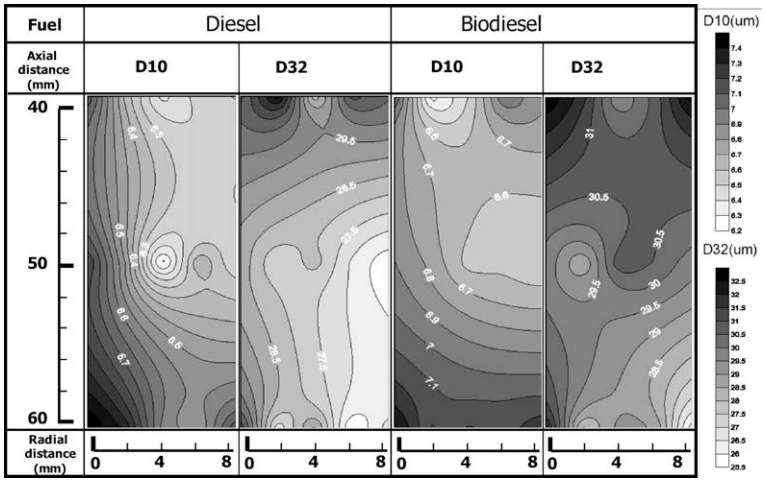


**Fig. 13.** Contour-plot of the mean droplet size distribution for the overall spray of diesel and biodiesel fuels ($P_{inj}$ = 60 MPa, $P_{amb}$ = 0.1 MPa, $t_{eng}$ = 1.2 ms).

creased tendency at a downstream of spray, because the atomization process of injected fuel from the injector is progressing by the drag force caused from the relative velocity between the ambient gas and injected fuel. Moreover, it can be confirmed that the atomization is more active at the outside of spray compared to the spray axis because of the increase of mixed area between fuel and ambient gas. On the other hand, biodiesel fuel with a higher viscosity has a lower droplet velocity than that of diesel fuel, after injection (Fig. 7b), and has worse volatility characteristics. From these reasons, biodiesel fuel has a higher SMD than diesel fuel at the whole spray region.

## 5. Conclusions

In this study, the spray and atomization characteristics of an undiluted biodiesel fuel were investigated, both experimentally and theoretically. The spray tip penetration, spray area and centroid variation were analyzed using a visualization system, while the droplet size and droplet distribution were obtained using a droplet measuring system. A numerical study was also performed using KIVA-3V code, and the calculated results were compared with the experimental results, including the spray tip penetration, the SMD distribution of the droplets, and the overall SMD. The conclusions from the experimental and numerical analyses performed in this study are summarized as follows.

As the injection pressure increases, the injection delay decreased due to the increase of fuel momentum by injection pressure, and the real injection duration increased about 30% compared to the energizing duration because of the response time of the injector solenoid from the injector driver. In addition, the volumetric injection rate of biodiesel fuel is lower than that of diesel fuel due to the higher dynamic viscosity and density of the fuel.

The spray tip penetration of biodiesel fuel has almost similar behavior pattern and its value compared with that of diesel fuel at various injection and ambient conditions. Moreover, the predicted spray tip penetration is in good agreement with the experimental results. The vortex shape of biodiesel fuel with high viscosity is clearer than that of diesel fuel because the breakup frequency of biodiesel fuel is low.

The spray area of biodiesel fuel decreases when the ambient pressure increases immediately after the start of injection. This indicates that the dense gas resulting from the high ambient pressure resists the spray development. It was also confirmed that the gradient in the spray centroid of the *Y*-axis tapers off as the ambient pressure increases.

The SMD of biodiesel fuel decreases along the spray axis. This is why the interaction between the spray and the ambient gas affects the fuel atomization. Biodiesel fuel has a slightly larger droplet size than diesel fuel. However the difference between the two fuels is small. In addition, the predicted local and overall SMD distribution for both diesel and biodiesel fuel are in good agreement with the experimental droplet size distribution. It needs to use the blended fuel between biodiesel and other fuel with low viscosity and good volatility in a diesel engine.

## Acknowledgement

This work was supported by the CEFV (Center for Environmentally Friendly Vehicle) of the Eco-STAR project of the MOE (Ministry of the Environment in Seoul, Republic of Korea). Also, this study was supported by the Second Brain Korea 21 Project in 2006.

## References

Bayvel, L., Orxechowski, Z., 1993. Liquid Atomization. Taylor&Francis, Washington, USA.
Beale, J.C., Reitz, R.D., 1999. Modeling spray atomization with the Kelvin–Helmholtz/Rayleigh–Taylor hybrid model. Atomization and Sprays 9, 623–650.
Bellman, R., Pennington, R.H., 1954. Effect of surface tension and viscosity on Taylor instability. Quarterly of Applied Mechanics 12, 151–162.
Bosch, W., 1966. The fuel rate indicator: a new measuring instrument for display of the characteristics of individual injection. SAE Technical Paper, 660–749.
Ejim, C.E., Fleck, B.A., 2007. Analytical study for atomization of biodiesels and their blends in a typical injector: surface tension and viscosity effects. Fuel 86, 1534–1544.
Hong, C., Choi, W., Choi, B., Lee, G., 2003. Characteristics of high pressure bio-diesel fuel spray. Transaction of KSAE 11 (2), 56–62.
Kegl, B., Kegl, M., Pehan, S., 2008. Optimization of a fuel injection system for diesel and biodiesel usage. Energy & Fuels 22, 1046–1054.
Kim, M.Y., Yoon, S.H., Lee, C.S., 2008. Impact of split injection strategy on the exhaust emissions and soot particulates from a compression ignition engine fueled with neat biodiesel. Energy & Fuels 22, 1260–1265.
Lee, C.S., Park, S.W., Kwon, S.I., 2005. An experimental study on the atomization and combustion characteristics of biodiesel-blended fuels. Energy & Fuels 19, 2201–2208.
Park, S.H., Suh, H.K., Lee, C.S., 2008. Effect of cavitating flow on the flow and fuel atomization characteristics of biodiesel and diesel fuels. Energy & Fuels 22 (1), 605–613.
Park, S.W., Bang, S.H., Lee, K.H., Lee, C.S., Lee, J. H., 2003. Atomization characteristics of common-rail diesel injector with multi-hole, SAE Technical Paper, 2003-01-1833.
Park, S.W., 2005. An internal structure and atomization characteristics of high pressure injection diesel sprays, Ph.D. Dissertation.
Payri, F., Bermudex, V., Payri, R., Salvador, F.J., 2004. The influence of cavitation on the internal flow and the spray characteristics in diesel injection nozzles. Fuel 83, 419–431.
Reitz, R.D., 1987. Modeling atomization processes in high-pressure vaporizing sprays. Atomization and Spray Technology 3, 309–337.

Roisman, I.V., Araneo, L., Tropea, C., 2007. Effect of ambient pressure on penetration of a diesel spray. International Journal of Multiphase Flow 33, 904–920.

Sarre, C.K., Kong, S., Reitz, R.D., 1999. Modeling the effect of injector nozzle geometry on diesel sprays, SAE Technical Paper, 1999-01-0912.

Schonborn, A., Ladommatos, N., Allan, R., Williams, J., Rogerson, J., 2008. Effect of the molecular structure of individual fatty acid alcohol esters (Biodiesel) on the formation of $NO_x$ and particulate matter in the diesel combustion process, SAE Technical Paper, 2008-01-1578.

Song, K.K., Sim, S.C., Jung, B.K., Kim, H.G., Kim, J.H., 2005. Effect of the injection parameters on diesel spray characteristics. KSME International Journal 19 (6), 1321–1328.

Su, T.F., Patterson, R.D., Reitz, R.D., Farrell, P.V., 1996. Experimental and numerical studies of high pressure multiple injection sprays, SAE Technical Paper, 960861.

Suh, H.K., Roh, H.G., Lee, C.S., 2008. Spray and combustion characteristics of biodiesel/diesel blended fuel in a direct injection common-rail diesel engine. Journal of Engineering for Gas Turbines and Power 130, 032807.

Yi, Y., Reitz, R.D., 2003. Modeling the effect of primary atomization on diesel engine emissions, SAE Technical Paper, 2003-01-1041.

Yoon, S.H., Park, S.H., Lee, C.S., 2008. Experimental investigation on the fuel properties of biodiesel and its blends at various temperature. Energy & Fuels 22 (1), 652–656.